AIP Advances

RESEARCH ARTICLE | MARCH 10 2021

In situ spectroscopic ellipsometry as a pathway toward achieving VO_2 stoichiometry for amorphous vanadium oxide with magnetron sputtering

C. Xu ; F. Heinemeyer ; A. Dittrich ; C. Bäumer ; R. Reineke-Koch

AIP Advances 11, 035126 (2021)
https://doi.org/10.1063/5.0041116

CrossMark

20 March 2024 09:24:29

In situ spectroscopic ellipsometry as a pathway toward achieving VO_2 stoichiometry for amorphous vanadium oxide with magnetron sputtering

Cite as: AIP Advances 11, 035126 (2021); doi: 10.1063/5.0041116
Submitted: 10 January 2021 • Accepted: 23 February 2021 •
Published Online: 10 March 2021

View Online

Export Citation

CrossMark

C. Xu,[1,a)] F. Heinemeyer,[1] A. Dittrich,[1] C. Bäumer,[2,3] and R. Reineke-Koch[1]

AFFILIATIONS

[1] Institute for Solar Energy Research Hamelin (ISFH), Am Ohrberg 1, 31860 Emmerthal, Germany
[2] Peter-Gruenberg Institute 7 and JARA-FIT, Forschungszentrum Juelich, 52428 Juelich, Germany
[3] MESA+ Institute for Nanotechnology, University of Twente, Faculty of Science and Technology, 7500 AE Enschede, The Netherlands

[a)] Author to whom correspondence should be addressed: c.xu@isfh.de

20 March 2024 09:24:29

ABSTRACT

As a special class of materials, transition metal oxides exhibit in their crystalline phase a variety of interesting properties, such as metal–insulator transition, ferroelectricity, magnetism, superconductivity, and so forth. However, for industrially widely applied methods such as room temperature magnetron sputtering, during initial fabrication steps of these materials, they are mostly amorphous, and control of stoichiometry during fabrication is challenging. It is, therefore, of pivotal importance to control the stoichiometry of transition metal oxides during growth in the amorphous state. One particularly important example for the necessity of stoichiometry control is vanadium dioxide (VO_2), where small deviations in stoichiometry during fabrication result in unfavorable changes in the electronic and structural properties, for example, the metal–insulator transition temperature and optical permittivity. In this work, the stoichiometry of amorphous vanadium oxides is adjusted to VO_2 using *in situ* spectroscopic ellipsometry (*in situ* SE) and verified by x-ray photoelectron spectroscopy. After an annealing process, a monoclinic VO_2 crystalline structure is observed through x-ray diffraction at 30 °C. At an elevated temperature of 150 °C, which is higher than the typical metal–insulator transition temperature in VO_2 of around 67 °C, a rutile crystalline structure is observed, which verifies the correctness of the stoichiometry of VO_2. A Mott metal–insulator transition is revealed by the change in the imaginary part of optical permittivity through SE as well.

© 2021 Author(s). All article content, except where otherwise noted, is licensed under a Creative Commons Attribution (CC BY) license (http://creativecommons.org/licenses/by/4.0/). https://doi.org/10.1063/5.0041116

Transition metal oxides exhibit various properties such as metal–insulator transition (MIT), ferroelectricity, and magnetism due to their unpaired electrons in the metal ion orbitals. However, these properties may disappear at their amorphous state. For specific applications, some certain valence states of the ions are desired. For example, with one electron in the d-orbital of the vanadium ion, named the d^1 electron configuration, VO_2 exhibits a Mott MIT from the insulating monoclinic phase to the metallic rutile phase at around 67 °C or 340 K, whereas the d^0-electron configuration in V_2O_5 and d^2 electron configuration in V_2O_3 exhibit no such phase changes at or above room temperature.[1–4] For thermochromic applications such as smart windows[3] or thermochromic solar absorbers close to room temperature,[5] the VO_2 stoichiometry is, therefore, mandatory, but the stoichiometry control during film growth is difficult. This leads to the high cost of adjusting and readjusting the fabrication parameters for a reproducible VO_2 phase.[6] If the growth temperature is sufficient for crystallization, an *in situ* analysis such as *in situ* x-ray diffraction (XRD) on vanadium oxides is possible.[7] However, as for the industrially widely applied methods such as room temperature magnetron sputtering,[8,9] where the vanadium

oxide remains amorphous during deposition, XRD methods fail to work. An *in situ* analysis tool is needed to provide real-time analytics of the amorphous vanadium oxide (VO_x) film properties to optimize the growth process in general and to achieve the targeted VO_2 composition reliably.

In this work, we demonstrate that *in situ* spectroscopic ellipsometry (*in situ* SE) is a sensitive analysis tool that may close this gap. *In situ* SE tracks the optical properties during the growth process,[10] which are closely linked to the stoichiometry induced band structure change.[11] We, therefore, succeeded in tracking the VO_x stoichiometry at various growth stages during growth, as also confirmed by *ex-situ* x-ray photoelectron spectroscopy (XPS). After annealing, these films of a well-defined composition exhibit the desired monoclinic to rutile phase transition and Mott MIT. Our work thus introduces *in situ* spectroscopic ellipsometry for stoichiometry monitoring during amorphous transition oxide thin film growth.

Three types of VO_x thin films, purchased from Sindlhauser Materials©;R and with a purity of 99.95%, were reactively sputtered from a vanadium target under an Ar background flux of 50 SCCM and 4.23×10^{-3} mbar total pressure, while the reactive gas O_2 fluxes were 1.4 SCCM (sample A1), 1.9 SCCM (sample B1), and 2.7 SCCM (sample C1). *In situ* SE measurements were performed with a SENTECH ellipsometer, in an energy range from 0.4 to 5.2 eV with a data acquisition time of around 300 s for each measurement. The spectral resolution in the range from 0.4 to 1.24 eV is 0.0038 eV, while the spectral resolution from 1.24 to 5.2 eV ranges from 0.005 to 0.01 eV. By modeling the ellipsometric parameters, namely, the amplitude ratio Ψ and the phase shift Δ between complex p- and s-polarization reflectivity from the *in situ* SE measurements, the imaginary part of the optical permittivity of the three types of samples with similar thicknesses of around 120 nm is as that summarized in Fig. 1(a). An increased infrared (IR) absorption in sample A1 is observed in comparison to sample B1. In contrast, the sample grown under the most oxidizing conditions (C1) reveals substantially lower absorption below 3 eV. A detailed analysis of the *in situ* SE data from sample B1 indicates an optical bandgap around 0.23 eV; however, sample A1 shows no optical bandgap, and sample C1 shows an optical bandgap higher than 1.5 eV (a detailed analysis of *in situ* SE data can be found in Sec. 2.1 of the supplementary material). In the literature, the crystalline, monoclinic M1-VO_2 phase has a bandgap between ~0.5[12] and 0.6 eV;[13,14] however, V_2O_3 is conductive at room temperature,[12] and V_2O_5 typically has a bandgap higher than 2 eV.[15] Therefore, samples A1 and C1 represent the most reduced and the most oxidized samples, respectively, and we tentatively assign the amorphous sample B1 to a composition of approximately VO_2, also considering the typical bandgap reduction in amorphous materials as demonstrated, for example, for Si.[16]

To verify this assignment, we performed XPS analysis using a PHI 5000 Versa Probe (Physical Electronics Inc., USA) with Al Kα x-ray illumination on identical samples fabricated with 1.4 SCCM (sample A2), 1.9 SCCM (sample B2) and 2.7 SCCM (sample C2), as shown in Fig. 1(b). The energy scale was calibrated with the carbon peak (C1s) at 284.8 eV and the oxygen peak (O1s) at 530 eV, and the V2p3/2 spectrum was fitted with multiple components—V^{5+} at 517.0 eV, V^{4+} at 516.1 eV, V^{3+} at 515.1 eV, V^{2+} at 513.6 eV, and V^{0+} at 512.3 eV—as suggested by comparative XPS works in the literature.[17] We note that all samples required several oxidation states,

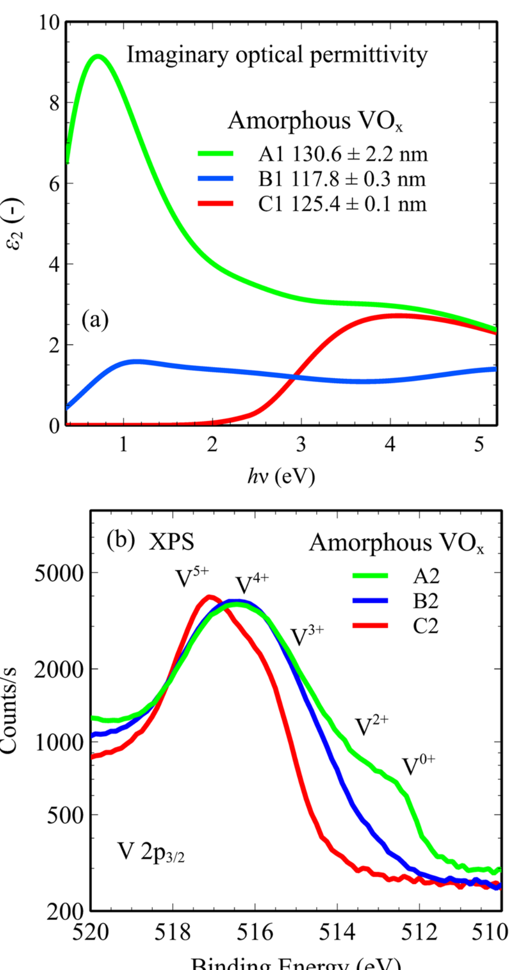

FIG. 1. (a) Fitted imaginary optical permittivity of A1, B1, and C1 samples during the deposition at the growth stage with around 120 nm layer thickness. (b) The XPS data for A2, B2, and C2 samples.

indicating a mixed valence state. However, the overall observation from XPS also supports our tentative assignment from *in situ* SE: the vanadium spectrum (V2p3/2) of sample B2 shows the highest V^{4+} fraction, while sample C2 has more V^{5+}. The V^{4+} fraction in A2, B2, and C2 is 40.4% ± 4%, 47.2% ± 5%, and 35.3% ± 4%, respectively. Sample A2 of the VO_x film with the lowest oxygen supply shows increased V^{3+}, V^{2+}, and even V^{0+} peaks. The oxygen flux chosen for samples B1 and B2, therefore, resulted in the targeted stoichiometry close to VO_2 (a detailed analysis of XPS spectra can be found in Sec. 1 of the supplementary material.)

During the growth, the amorphous B1 thin film exhibits varying optical properties. By modeling the Ψ and Δ data from the *in situ* SE measurements with WVASE© [Figs. 2(a) and 2(b)], the imaginary part of optical permittivity is as summarized in Fig. 2(c). The Ψ and Δ data in the measurement range are well fitted with a combined model of one Tauc–Lorentz oscillator and two Gaussian oscillators (a detailed analysis of the *in situ* SE data is given

20 March 2024 09:24:29

© Author(s) 2021

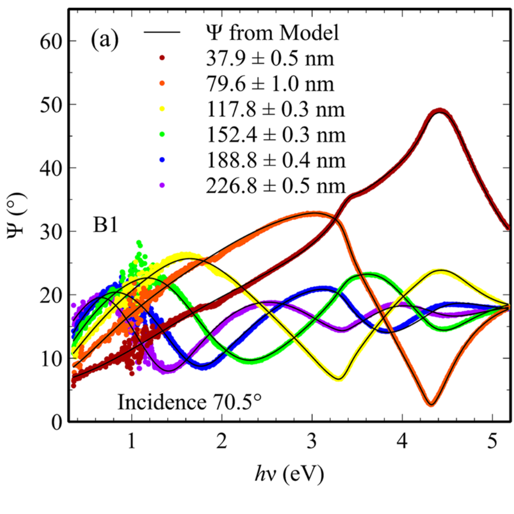

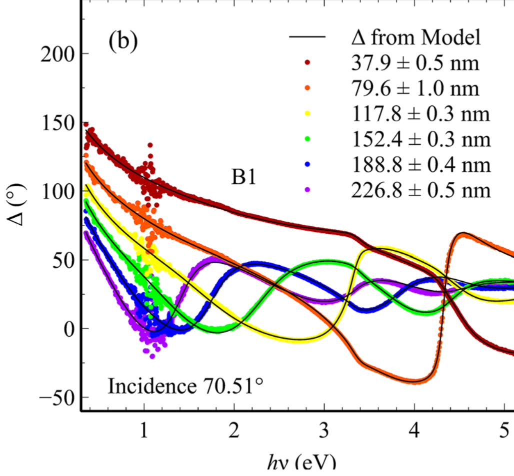

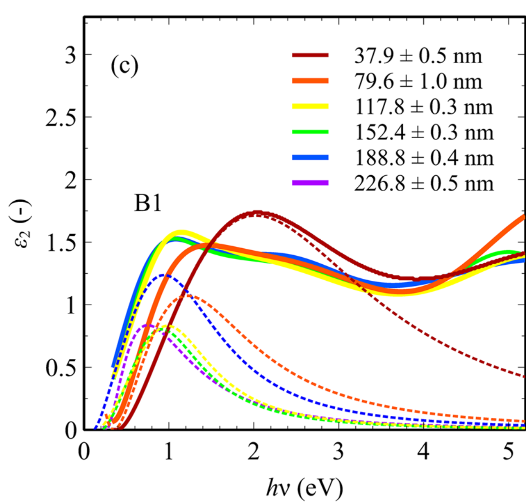

FIG. 2. Comparison of the model (black lines) and experimental data (colored dots) in (a) the Ψ data and (b) Δ data for *in situ* SE in sample B1. (c) The experimental data (colored lines) of the imaginary optical permittivity (ε_2) during growth of sample B1 and the Tauc–Lorentz oscillator (broken lines) near the bandgap.

in Sec. 2.2 in the supplementary material). As a guide to the naked eye, the contribution from the Tauc–Lorentz oscillator at different growth stages is presented as a broken line in Fig. 2(c), from which the change in bandgap is obvious. A significant reduction in the bandgap from 0.39 ± 0.08 to 0.15 ± 0.05 eV is observed at the initial growth stage from 28.4 to 117.6 nm, while all thicker films had a bandgap above 0.1 eV. The high bandgap at the initial growth stage might originate from the compressive strain,[18] which relaxes as the film thickness increases. Alternatively, a quantum size effect could cause a larger bandgap at the beginning of the layer growth, which has been observed in other oxide materials such as TiO_2.[19] *In situ* SE delivers, thus, the information not only after growth but also during the growth at various stages and reveals the important changes such as optical bandgaps. This is important for understanding the general growth processes.

Next, we studied the crystallization of the thin film B1 by annealing in an x-ray diffraction setup. Prior to any annealing process, the sample is measured in an X'pert Panalytical XRD analyzer with grazing incidence x-ray diffraction (GIXRD) at an incidence angle of 1°. After a 10 min annealing process at 500 °C under 10^{-2} mbar with ambient air in the graphite chamber, sample B1 is cooled down and measured with GIXRD with the same parameters. While the as-grown thin film B1 shows an amorphous structure, after annealing, the diffraction peaks suggesting a monoclinic VO_2 phase (M1-VO_2)[20] are observed in sample B1 measured at 30 °C. As suggested by the literature, some anodized VO_x films showing undiscernible XRD peaks could show phase transition as well,[21] indicating small and highly defective crystallites of VO_2. However, this should not be the case in our samples since we have not observed any phase transition at the as-deposited state by optical measurements. Hence, the samples are not only x-ray amorphous but also amorphous with respect to phase transition. At an elevated temperature of 150 °C, sample B1 exhibits diffraction peaks that can be attributed to a rutile VO_2 phase (R-VO_2)[22] (Fig. 3). Although small deviations between

20 March 2024 09:24:29

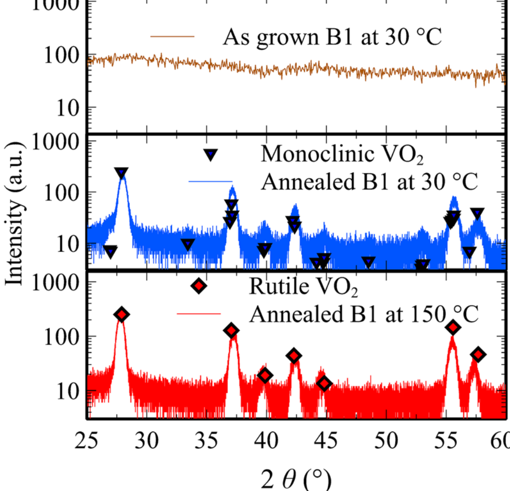

FIG. 3. GIXRD measurement of the as-grown B1 sample measured at 30 °C (upper), the annealed B1 sample measured at 30 °C (middle), and the annealed B1 sample at 150 °C (lower).

© Author(s) 2021

the measured peak positions and the literature are observed, the main distinction between monoclinic and rutile structures, which is the increased number of diffraction peaks in the monoclinic VO_2 phase due to lower symmetry, is observed. The rutile structure can be reversibly turned to monoclinic upon cooling to 30 °C (not shown here). The crystalline VO_2 samples, however, should be crystallized in small crystallites. That is the reason why they show low XRD peak intensity. A detailed comparison between the measured peaks and peaks in the literature with $27° < 2\theta < 53°$ is presented in Table I.

We also verified the Mott MIT through the imaginary part of optical permittivity. After the deposition, the as-grown B1 thin film has been characterized with *ex-situ* SE at 25 °C. After annealing in XRD at 500 °C, *ex-situ* SE measurements are carried out between 25 °C and 150 °C. The incidence angles are 40°, 50°, 60°, 70°, and 80°. The spectral range of *ex-situ* SE is 0.04–5.2 eV. The UV–Vis part of the measurement between 0.74 and 5.2 eV is performed on a J.A. Woollam M2000©, and the infrared part from 0.032 to 0.74 eV is carried out on the J.A. Woollam IR-VASE© equipment. The spectral resolution of *ex-situ* SE is 0.0038 eV from 0.032 to 0.74 eV, while the spectral resolution lies between 0.0006 and 0.01 eV from 0.74 to 5.2 eV. The fitted results to each measurement are summarized in the form of the imaginary part of optical permittivity, while the error bars for all fits are supplied in the supplementary material.

The imaginary part of the optical permittivity (ε_2) of as-grown and annealed B1 from *in situ* SE and *ex-situ* SE is compared in Fig. 4(a). By comparing the as-grown B1 measured by *in situ* SE (blue curve) and *ex-situ* SE (black curve), we see, in general, reduced absorption in the visible–UV range, which is in good accordance with the literature and may be caused by oxygen absorption on the sample surface.[23] The annealed B1 sample shows two types of peaks at 25 °C: (1) the peaks with energy above the optical bandgap of around 0.6 eV in VO_2 show typical optical permittivity as the crystalline M1 monoclinic VO_2 phase in the literature,[12,24] where three characteristic peaks are observed (a detailed analysis for peaks is supplied Sec. 2.3 in the supplementary material): (1a) the peak position around 1.2 eV corresponds to transition from the filled a_{1g} to the empty e_g^{π} band, (1b) the peak position around 2.3 eV refers to the transition from the filled a_{1g} to the empty a_{1g}^* band, and (1c) the peak position around 3.4 eV corresponds to the transition from the filled O_{2p} bands to the empty $e_g^{\pi *}$ band. (2) The peak with energy below the optical bandgap of around 0.6 eV in VO_2 suggests the existence of defects. The peak around 74 meV may correspond to defects such as oxygen deficiencies in the VO_2 thin film.[25] At 150 °C, the annealed B1 shows the typical feature of rutile VO_2[12]: two peaks at 2.6 and 3.4 eV merge into a broad peak, while a strong absorption appears in the infrared range. The as-grown B1 shows smeared and suppressed peaks in the ultraviolet to visible range, while a peak at 66 ± 0.2 meV is observed as well. Moreover, the bandgap (E_g) of the annealed B1 sample at 25 °C is 0.45 ± 0.01 eV, while the as-grown B1 shows E_g = 0.077 ± 0.063 eV that is much lower even with regard to the error level. This measurement deviates from E_g = 0.26 ± 0.04 eV by *in situ* SE, which may be attributed to the oxygen absorbents suggested by Motyka[23] or carbon absorbents that are verified by the XPS C1s peak. Amorphous VO_2 has been studied by *in situ* SE by Podraza *et al.*[26] They observe high absorption close to 0.7 eV in amorphous VO_x with $2 < x < 2.5$, which inhibits quantitative determination of the optical bandgap. We also observe high absorption even down to 0.7 eV in amorphous VO_x by both *in situ* SE and *ex-situ* SE. This high absorption at 0.7 eV, however, could be interpreted as an effect of two overlapping peaks: one Tauc–Lorentz peak of amorphous VO_2 as discussed above and one Lorentz peak originating from the possible oxygen vacancy level(s). The bandgap of the annealed B1 sample is just slightly lower than other experimental optical bandgaps of crystalline M1-VO_2 with values between 0.5[12] and 0.6 eV,[14] which might be attributed to the oxygen vacancies that could lead to reduction in bandgap.[27] The reduction in bandgap from the crystalline to the amorphous phase has been observed also for other materials such as Si.[16] By heating and cooling the annealed sample B1 with finer steps, a clear Mott MIT with increased IR absorption can be observed around 67 °C upon heating, while the absorption is reduced at around 55 °C during cooling [Fig. 4(b)]. With regard to the amplitude of Drude oscillators applied for the fits, which represent the infrared absorption due to the metallic rutile phase in the annealed B1 samples, a clear hysteresis is observed during the heating and cooling processes [Fig. 4(c)]. The Mott MIT is thus verified in the annealed B1 sample with complete features of VO_2, again confirming that our *in situ* SE monitoring enabled deposition with close-to-correct stoichiometry.

TABLE I. Comparison of the measured XRD peaks in the range of $27° < 2\theta < 53°$ with known data from the literature including Miller indices.[20,22]

	XRD peak position (°) with Miller indices							
Monoclinic[20]	27.9 (1 1 −1)	33.4 (1 0 −2)	37.1 (1 1 1)	39.8 (2 0 −2)	42.4 (0 1−2)	44.8 (1 2 −1)	48.5 (1 0 2)	53.0 (1 2 −2)
Annealed B1 @ 30 °C	28.0	33.6	37.2	39.8	42.4	44.9	48.4	53.0
Rutile[22]	27.9 (1 1 0)		37.1 (1 0 1)	39.9 (2 0 0)	42.3 (1 1 1)	44.8 (2 1 0)		
Annealed B1 @ 150 °C	27.8		37.2	39.7	42.4	44.6		

20 March 2024 09:24:29

© Author(s) 2021

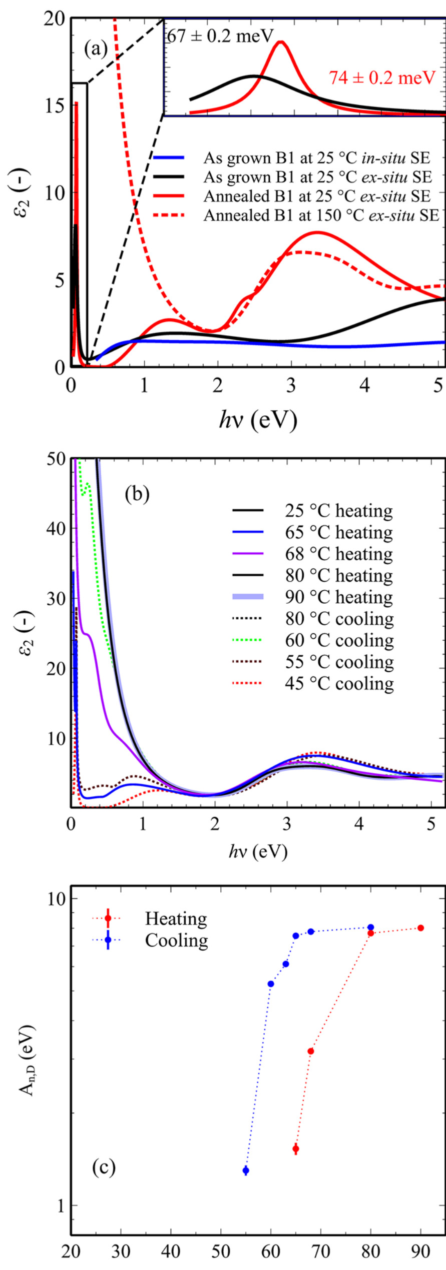

FIG. 4. (a) Imaginary part of optical permittivity from *in situ* spectroscopic ellipsometry on the as-grown B1 sample measured at 25 °C (blue, solid), *ex-situ* spectroscopic ellipsometry on the as-grown B1 sample measured at 25 °C (black), the annealed B1 sample measured at 25 °C (red, solid), and the annealed B1 sample measured at 150 °C (red, broken). The inset shows an enlarged view of the as-grown B1 sample and annealed B1 sample measured at 25 °C in a range from 20 to 150 meV. (b) The temperature dependence of the imaginary part of optical permittivity in the annealed B1 sample ranging from 0.032 to 5.2 eV from 25 °C to 90 °C with both heating and cooling cycles. (c) The fitted amplitude of the Drude oscillator from 25 °C to 90 °C as an indicator of the infrared absorption in the logarithmic scale. Below 65 °C by heating and below 55 °C by cooling, no Drude oscillators are applied. The values of the error bars are supplied in the supplementary material.

To summarize, the stoichiometry of amorphous VO_x thin films can be observed by *in situ* spectroscopic ellipsometry. We used *in situ* SE to distinguish three stoichiometries and determined the growth parameters to deposit the intended VO_2 layer, as verified by XPS. The close to ideal stoichiometry of the as-deposited, amorphous layer leads to a monoclinic VO_2 phase after a short annealing process, which shows a Mott metal–insulator transition. *In situ* spectroscopic ellipsometry can thus be applied to control stoichiometry in mass-scalable fabrication processes of amorphous transition metal oxides.

See the supplementary material for the complete analysis of XPS data and *in situ* and *ex-situ* spectroscopic ellipsometry data.

Part of the presented work was funded by the German Federal Ministry for Economic Affairs and Energy, under Contract No. 0325858 A and B in accordance with a decision of the German Federal Parliament. This project was carried out in cooperation with the company Viessmann Werke GmbH and Co. KG. We thank Professor Regina Dittmann for scientific discussions and access to the electronic-oxide-UHV-cluster-tool at Forschungszentrum Jülich.

DATA AVAILABILITY

The data that support the findings of this study are available from the corresponding author upon reasonable request.

REFERENCES

[1] M. E. A. Warwick and R. Binions, J. Mater. Chem. A **2**, 3275 (2014).

[2] M. Brahlek, L. Zhang, J. Lapano, H.-T. Zhang, R. Engel-Herbert, N. Shukla, S. Datta, H. Paik, and D. G. Schlom, MRS Commun. **7**, 27 (2017).

[3] Y. Cui, Y. Ke, C. Liu, Z. Chen, N. Wang, L. Zhang, Y. Zhou, S. Wang, Y. Gao, and Y. Long, Joule **2**, 1707 (2018).

[4] T.-C. Chang, X. Cao, S.-H. Bao, S.-D. Ji, H.-J. Luo, and P. Jin, Adv. Manuf. **6**, 1 (2018).

[5] D. Mercs, A. Didelot, F. Capon, J.-F. Pierson, B. Hafner, A. Pazidis, S. Föste, and R. Reineke-Koch, Energy Procedia **91**, 84 (2016).

[6] D. Bhardwaj, D. K. Singh, S. B. Krupanidhi, and A. M. Umarji, Appl. Phys. A **126**, 157 (2020).

[7] G. Rampelberg, B. De Schutter, W. Devulder, K. Martens, I. Radu, and C. Detavernier, J. Mater. Chem. C **3**, 11357 (2015).

[8] M. Kharrazi Olsson, K. Macák, and W. Graf, Surf. Coat. Technol. **122**, 202 (1999).

[9] M. Braun, in *Handbook of Manufacturing Engineering and Technology*, edited by A. Y. C. Nee (Springer London, London, 2015), pp. 2929–2957.

[10] U. Kilic, A. Mock, D. Sekora, S. Gilbert, S. Valloppilly, N. Ianno, M. Langell, E. Schubert, and M. Schubert, Sci. Rep. **10**, 10392 (2020).

[11] E. Langereis, H. C. M. Knoops, A. J. M. Mackus, F. Roozeboom, M. C. M. van de Sanden, and W. M. M. Kessels, J. Appl. Phys. **102**, 083517 (2007).

[12] M. M. Qazilbash, A. A. Schafgans, K. S. Burch, S. J. Yun, B. G. Chae, B. J. Kim, H. T. Kim, and D. N. Basov, Phys. Rev. B **77**, 115121 (2008).

[13] H. W. Verleur, A. S. Barker, and C. N. Berglund, Phys. Rev. **172**, 788 (1968).

[14] S. Lee, T. L. Meyer, C. Sohn, D. Lee, J. Nichols, D. Lee, S. S. A. Seo, J. W. Freeland, T. W. Noh, and H. N. Lee, APL Mater. **3**, 126109 (2015).

[15] C. Lamsal and N. M. Ravindra, J. Mater. Sci. **48**, 6341 (2013).

[16] P. K. Giri, S. Tripurasundari, G. Raghavan, B. K. Panigrahi, P. Magudapathy, K. G. M. Nair, and A. K. Tyagi, J. Appl. Phys. **90**, 659 (2001).

[17] G. Silversmit, D. Depla, H. Poelman, G. B. Marin, and R. De Gryse, J. Electron Spectrosc. Relat. Phenom. **135**, 167 (2004).

[18] B. Lazarovits, K. Kim, K. Haule, and G. Kotliar, Phys. Rev. B **81**, 115117 (2010).

20 March 2024 09:24:29

© Author(s) 2021

[19]H. Lin, C. P. Huang, W. Li, C. Ni, S. I. Shah, and Y.-H. Tseng, Appl. Catal., B **68**, 1 (2006).
[20]R. W. G. Wyckoff, *Crystal Structures* (Interscience Publishers, New York, 1982).
[21]G. B. Stefanovich, A. L. Pergament, A. A. Velichko, and L. A. Stefanovich, J. Phys.: Condens. Matter **16**, 4013 (2004).
[22]H. R. Hoekstra, S. Siegel, and F. X. Gallagher, Platin. Gr. Met. Compd. **98**, 4 (1971).
[23]M. A. Motyka, B. D. Gauntt, M. W. Horn, E. C. Dickey, and N. J. Podraza, J. Appl. Phys. **112**, 093504 (2012).
[24]T. J. Huffman, C. Hendriks, E. J. Walter, J. Yoon, H. Ju, R. Smith, G. L. Carr, H. Krakauer, and M. M. Qazilbash, Phys. Rev. B **95**, 75125 (2017).
[25]C. Chen, Y. Zhao, X. Pan, V. Kuryatkov, A. Bernussi, M. Holtz, and Z. Fan, J. Appl. Phys. **110**, 023707 (2011).
[26]N. J. Podraza, B. D. Gauntt, M. A. Motyka, E. C. Dickey, and M. W. Horn, J. Appl. Phys. **111**, 073522 (2012).
[27]L. Fan, X. Wang, F. Wang, Q. Zhang, L. Zhu, Q. Meng, B. Wang, Z. Zhang, and C. Zou, RSC Adv. **8**, 19151 (2018).

20 March 2024 09:24:29

© Author(s) 2021